# Optical Spectroscopy and Visible Upconversion Studies of $YVO_4:Er^{3+}$ Nanocrystals Synthesized by a Hydrothermal Process

Yajuan Sun,[†] Hongjian Liu,[‡] Xin Wang,[†] Xianggui Kong,*[,†] and Hong Zhang*[,§]

*Key Laboratory of Excited-State Processes, Changchun Institute of Optics Fine Mechanics and Physics, Chinese Academy of Sciences, Changchun 130033, P. R. China, Quantum Dot Corporation, 26118 Research Road, Hayward, California 94545, and Van't Hoff Institute for Molecular Science, University of Amsterdam, Nieuwe Achtergracht 166, 1018 WS Amsterdam, The Netherlands*

*Received September 1, 2005. Revised Manuscript Received November 28, 2005*

Strong visible emissions of $Er^{3+}$ resulting from two-photon absorption and energy transfer from the host $YVO_4$ were observed in nanocrystalline $Er^{3+}$-doped $YVO_4$, which was prepared by a hydrothermal method using a citrate−yttrium−vanadate complex as the precursor. The nanocrystals were characterized using X-ray diffraction (XRD), Fourier transform infrared spectroscopy (FT-IR), transmission electron microscopy (TEM), UV−visible absorption spectra, and photoluminescence (PL) spectra. The highly crystalline $YVO_4:Er^{3+}$ nanoparticles, with an average diameter of 35 nm, have a tetragonal zircon structure and can redisperse in water because of the presence of citrate ligands. We discussed in detail the visible upconversion mechanism and temperature dependence of the upconversion emission for the $Er^{3+}$ ions in the $YVO_4$ nanocrystals.

## Introduction

Rare-earth-doped luminescence materials have wide applications, including phosphors, display monitors, X-ray imaging, scintillators, lasers, and amplifiers for fiber-optic communications.[1−7] The luminescence efficiency of these materials is often limited by the dynamics of the rare-earth (RE) ion, which depends on the interaction between RE ions and the host.[8] Among many RE ions, trivalent erbium ion is well-known as an active dopant for many different inorganic lattices, producing white-light emission by adjusting the ratio of blue, green, and red emissions.[9,10] In addition, an $Er^{3+}$ ion is particularly suitable for the upconversion of infrared to visible light because of a favorable electronic level scheme with equally spaced, long-lived excited states.

Fluorescence labeling on biomolecules is a very important practice in biological applications such as immunoassaying, DNA sequencing, and clinical diagnosing.[11−15] The challenge, however, is to identify or devise the high sensitivity, stability, security, and capacity to penetrate into cells. RE-doped upconverting phosphors have been reported to be used for the detection of nucleic acid and immunoassays.[16−18] As fluorescence labeling materials compared with conventional fluorophores (e.g., cy5),[19] upconverting phosphors (UCP) with no photobleaching and a lower background show a higher detection sensitivity when illuminated with infrared (IR) light (980 nm). This work is motivated by not only the application of the $Er^{3+}$-doped nanocrystals as UCP for fluorescence labeling but also the interest to better understand the luminescence properties of erbium in different hosts.

Yttrium orthovanadate ($YVO_4$) is well-known as a very attractive phosphor-producing host lattice for several metal ions, as the bulk materials exhibit a high luminescence efficiency.[20] For example, $Eu^{3+}$-ion activated $YVO_4$ can be utilized as a red phosphor in a cathode ray tube (CRT), and as a scintillator in medical image detectors.[21] Moreover, it performs as a promising polarizer and laser host material in

* To whom correspondence should be addressed. Tel: 86-431-6176313. Fax: 86-431-4627031. E-mail: xgkong14@ciomp.ac.cn (X.K.); Hong@science.uva.nl (H.Z.).

[†] Chinese Academy of Sciences.

[‡] Quantum Dot Corporation.

[§] University of Amsterdam.

(1) Blasse, G.; Grabmaier, B. C. *Luminescent Materials*; Springer-Verlag: Berlin, 1994.
(2) Denjeka, M. J.; Samson, B. *Mater. Res. Soc. Bull.* **1999**, *8*, 39.
(3) Reisfeld, R.; Jorgensen, C. K. *Lasers and Excited States of Rare Earths*; Springer-Verlag: Berlin, 1977.
(4) Mehta, A.; Thundat, T.; Barnes, M. D.; Chhabra, V.; Bhargava, R.; Bartko, A. P.; Dickson, R. M. *Appl. Opt.* **2003**, *42*, 2132.
(5) Patra, A.; Friend, C. S.; Kapoor, R.; Prasad, P. N. *J. Phys. Chem. B* **2002**, *106*, 1909.
(6) Zhang, H. X.; Kam, C. H.; Zhou, Y.; Han, X. Q.; Buddhudu, S.; Xiang, Q.; Lam, Y. L.; Chan, Y. C. *Appl. Phys. Lett.* **2000**, *77*, 609.
(7) Uchida, A.; Yoshimori, S. *C. R. Phys.* **2004**, *5*, 643.
(8) Jia, W. Y.; Monge, K.; Fernandez, F. *Opt. Mater.* **2003**, *23*, 27.
(9) Capobianco, J. A.; Vetrone, F.; Boyer, J. C.; Speghini, A.; Bettinelli, M. *J. Phys. Chem. B* **2002**, *106*, 1181.
(10) Luo, L.; Zhang, X. X.; Li, K. F.; Cheah, K. W.; Shi, J. X.; Wong, W. K.; Gong, M. L. *Adv. Mater.* **2004**, *16*, 1664.
(11) Hsu, C.; Powell, R. C. *J. Lumin.* **1975**, *10*, 23.
(12) Wu, X. Y.; Liu, H. J.; Liu, J. Q.; Haley, K. N.; Treadway, J. A.; Larson, J. P.; Ge, N. F.; Peale, F.; Bruchez, M. P. *Nat. Biotechnol.* **2003**, *21*, 41.
(13) Chan, W. C.; Nie, S. M. *Science* **1998**, *281*, 2016.
(14) Santra, S.; Zhang, P.; Wang, K. M.; Tapec, R.; Tan, W. H. *Anal. Chem.* **2000**, *72*, 5748.
(15) Hampl, J.; Hall, M.; Mufti, N. A.; Yao, Y. M.; Macquee, D. B.; Wright, W. H.; Cooper, D. E. *Anal. Biochem.* **2001**, *288*, 176.
(16) Rijke, F. V. D.; Zijlmans, J.; Li, S.; Vail, T.; Raap, A. K.; Niedbala, R. S.; Tanke, H. J. *Nat. Biotechnol.* **2001**, *19*, 273.
(17) Beverloo, H. B.; Schadewijk, A.; Van, Zijlmans, H. J. M. A. A.; Tanke, H. J. *Anal. Biochem.* **1992**, *203*, 326.
(18) Niedbala, R. S.; Feindt, H.; Kardos, K.; Vail, T.; Burton, J.; Bielska, B.; Li, S.; Milunic, D.; Bourdelle, P.; Vallejo, R. *Anal. Biochem.* **2001**, *293*, 22.
(19) Schuler, B.; Pannell, L. K. *Bioconjugate Chem.* **2002**, *13*, 1039.
(20) Levine, A. K.; Palilla, F. C. *Appl. Phys. Lett.* **1964**, *5* (6), 118.
(21) Panayiotakis, G.; Cavouras, D.; Kandarakis, I.; Nomicos, C. *Appl. Phys. A* **1996**, *62*, 483.

10.1021/cm051971m CCC: $33.50 
Published on Web 05/02/2006

its single-crystal form.[22,23] $YVO_4$ can also be obtained in its crystallized form by precipitation reactions at low temperature without calcinations. Recently, various routes of the wet-chemical synthesis of RE-doped nanocrystals were reported by Haase et al. and Huignard et al.[24,25] The advantage of these methods is that the obtained nanoparticles are uniform in size and easily dispersible.

In this paper, we have successfully synthesized the water-soluble $Er^{3+}$-doped $YVO_4$ nanocrystals by a hydrothermal treatment, using citrate as a complexing agent. The nanocrystals perform a strong visible emission of $Er^{3+}$ under either infrared excitation via upconversion or the excitation of the host via an energy-transfer process from the host to $Er^{3+}$. The relevant properties are studied by different techniques, e.g., X-ray diffraction (XRD), Fourier transform infrared spectroscopy (FT-IR), transmission electron microscopy (TEM), UV−visible absorption spectroscopy, and emission spectroscopy.

## Experimental Section

**Material.** All reagents were analytical grade. $RE(NO_3)_3 \cdot 6H_2O$ (RE = Y and Er) salt was freshly prepared by the reaction of $RE_2O_3$ with nitric acid. Water was distilled and deionized using a Millipore Milli-Q Purification System, which has a resistivity of not less than 18.2 MΩ.

**Synthesis of $YVO_4$:Er Nanocrystals.** The synthesis of yttrium orthovanadate by aqueous precipitation reactions was reported in the work of Huignard and Buissette.[25] In the present work, improvements have been made to enhance the crystallizability of the particles. The procedure is as follows:

In a water bath at 60°C, an aqueous solution of $Y(NO_3)_3$ and $Er(NO_3)_3$ (10 mL, 0.1 M) was mixed with an aqueous solution of sodium citrate (7.5 mL, 0.1 M) under vigorous stirring, and a white precipitate of lanthanide citrate was formed. An aqueous solution of $Na_3VO_4$ (10 mL, 0.1 M, pH 13) was then added dropwise to the above mixture until the precipitate was completely dissolved. After being stirred for 1 h, the resulting clear precursor solution, with a pH of 8.0, was transferred to a 60 mL autoclave for hydrothermal treatment at 200 °C for 24 h. Naturally cooled to room temperature, the precipitate of $YVO_4$:Er nanocrystals in the autoclave could be separated from the reaction media by centrifugation (7000 rpm, 10 min) and then washed with deionized water several times. After being dried under vacuum at 40−50 °C, phosphor particles of $YVO_4$ doped with $Er^{3+}$ in nanometer size were obtained. For comparison, the prepared precursor solution was cooled and dialyzed against deionized water for 24 h;[25] it was then dried under vacuum at 40−50 °C. Colloidal suspensions of $YVO_4:Er^{3+}$ were obtained by ultrasonically redispersing dry nanocrystalline powders in deionized water. The samples that contained 2.0 mol % Er were used in this study.

**Characterization.** The structure and morphology of $YVO_4$:Er nanocrystals were characterized by XRD, FT-IR spectra, and TEM. XRD studies were performed on powders using a Japan Rigaku D/max-rA X-ray diffractometer system with monochromatized Cu Kα radiation ($\lambda$ = 1.5406 Å). FT-IR spectra were recorded on a Perkin-Elmer 580B infrared spectrophotometer with the KBr pellet technique. TEM observations were completed out on a Hitachi H-8100 IV microscope operating at 200 KV. High-resolution TEM (HRTEM) was obtained by using a JEOL 2010 microscope operating at 200 kV. For TEM observations, the products were ultrasonically dispersed in ethanol, and a drop of this solution was then placed on a Cu grid coated with a holey carbon film.

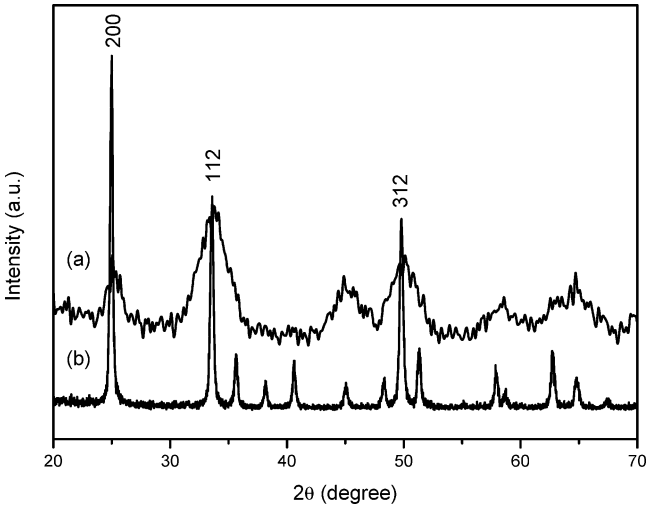


**Figure 1.** XRD patterns performed on a powder of the $YVO_4:Er^{3+}$ nanocrystals obtained (a) by drying the synthesized precursor and (b) after hydrothermal treatment.

UV−visible absorption and fluorescence emission spectra of the colloidal solutions were measured at room temperature with a UV-3000 spectrometer and a Hitachi F-4500 spectrofluorometer, respectively.

The upconversion emission spectra of $Er^{3+}$ in the $YVO_4$ nanocrystals were acquired using a Jobin−Yvon LabRam Raman spectrometer system equipped with 1800 and 600 grooves/mm holographic gratings and a Peltier air-cooled CCD detector. Precise control of the sample temperature (±0.1 °C) was achieved by means of a Linkam THMS600 temperature programmable heating/cooling microscope stage. The THMS stage was used in conjunction with a Linkam LNP cooling system when cooling. Samples were excited by a semiconductor diode laser with a 980 nm wavelength.

## Results and Discussion

**Structural and Morphological Investigations.** Figure 1 shows the XRD patterns of the nanocrystalline $YVO_4:Er^{3+}$ before and after hydrothermal treatment. All peaks can be indexed to the same tetragonal phase (JCPDS Card, File No. 17-0341) with a zircon-type structure as bulk $YVO_4$.[26,27] There is only one yttrium site in the unit cell, and the point symmetry of $Y^{3+}$ is $D_{2d}$, without an inversion center.[24] As the radius of $Er^{3+}$ (88.1 pm) is close to the radius of the $Y^{3+}$ (88 pm) ion, the erbium ion easily substitutes for yttrium in the $D_{2d}$ site of the yttrium vanadate lattice. Furthermore, the intensities of the main peaks evidently increase in reference to the background after hydrothermal treatment, and the full width at half-maximum (fwhm) of the peaks of the particles after hydrothermal treatment is smaller than those of the particles before hydrothermal treatment. This means the hydrothermal treatment efficiently increased the crystallinity. The size of the particles was also calculated using the Debye−Scherrer equation

$$D = \frac{K\lambda}{\beta \cos \theta} \quad (1)$$

(22) Maunders, E. A.; Deshazer, L. G. *J. Opt. Soc.* **1971**, *61*, 684.
(23) O'Connor, J. R. *Appl. Phys. Lett.* **1966**, *9*, 407.
(24) Riwotzki, K.; Haase, M. *J. Phys. Chem. B* **1998**, *102*, 10129.
(25) Huignard, A.; Buissette, V.; Laurent, G.; Gacoin, T.; Boilot, J. P. *Chem. Mater.* **2002**, *14*, 2264.

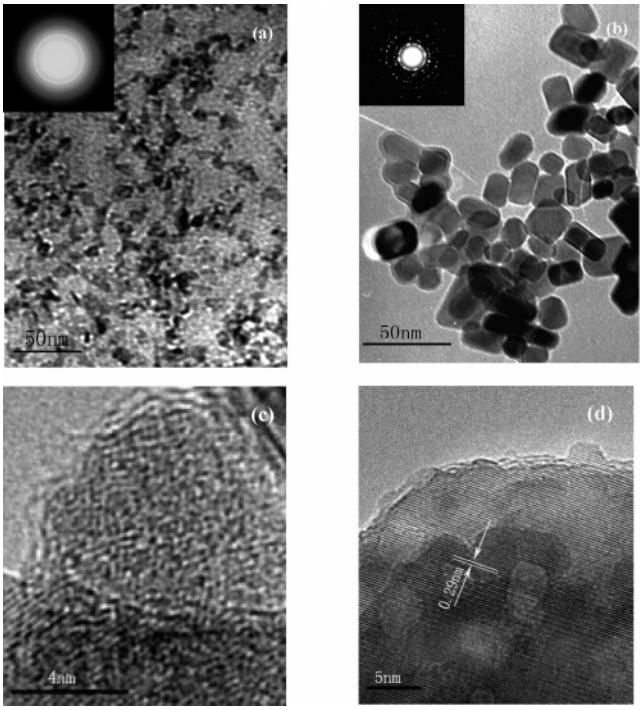


**Figure 2.** TEM images of (a) synthesized precursor and (b) nanocrystalline $YVO_4:Er^{3+}$ after hydrothermal treatment (inset displays the SAED pattern), and (c and d) high magnification of (a) and (b), respectively.

where $K = 0.89$, $D$ represents the crystallite size (Å), $\lambda$ is the wavelength of the Cu Kα radiation, $\theta$ is the Bragg angle of the peak, and $\beta$ is the measured fwhm of the diffraction peak. By applying the Debye−Scherrer formula to the (200) diffraction peaks, we determined the mean particle sizes of the precursor and final products to be 9 and 40 nm, respectively.

The morphologies of the particles before and after hydrothermal treatment were identified by TEM, as shown in Figure 2. It can be seen from the TEM images that the prepared precursor particles with a diameter of 7 nm show an irregular shape; it is evident that most of the particles after hydrothermal treatment are a tetragonal-like morphology with an average diameter of 35 nm in size, and few of them appear to be close in shape to that of a sphere. The TEM images show a smaller mean particle size than that estimated from the XRD patterns. This deviation comes from the fact that the particle size determined by the Scherrer equation is a volume-averaged size, whereas analysis of the TEM pictures typically leads to a number average of the particles. Therefore, a small number of large particles have a big contribution to the diffraction measurement. The selected area electron diffraction (SAED) pattern recorded for the colloidal precursor is composed of continuous rings, whereas the one after hydrothermal treatment shows some discrete spots. This demonstrates that both samples are polycrystalline and indicates that the average particle size increases because of the hydrothermal treatment, and the particle's crystallinity is expected to increase. High-resolution TEM images of the precursor particles and the hydrothermal images are shown in panels c and d of Figure 2, respectively. The precursor

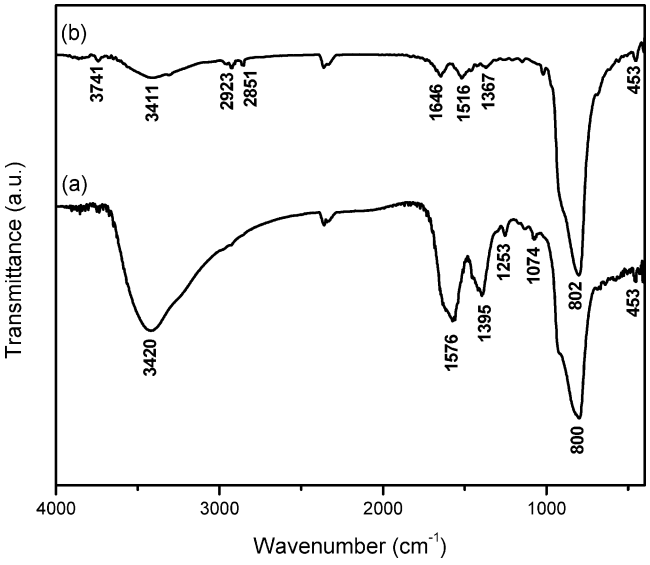


**Figure 3.** FT-IR spectra in KBr of the $YVO_4:Er$ powder (a) before and (b) after hydrothermal treatment.

particle shows unclear and curving lattice fringes, and the hydrothermal sample depicts well-defined lattice fringes (200) with 0.29 nm interplanar spacing. From the HRTEM image (Figure 2d), we can also see that the formation of the particles occurs through the aggregation of primary particles followed by the epitaxial fusing together. Furthermore, the contrast observed within both samples indicates that the precursor particles have numerous defects, and nanocrystals after hydrothermal treatment are structurally comparatively perfect. The defects of the precursor particles, we think, probably tend to migrate to the surface of the nanocrystal during the growth stage because of the hydrothermal process.

Figure 3 shows the FT-IR spectra of $YVO_4:Er^{3+}$ nanoparticles before and after hydrothermal treatment. From the FT-IR spectra, it can be observed that the strong peak at 800 $cm^{-1}$ and the weak peak at 453 $cm^{-1}$ are apparently associated with the characteristic vibrational mode of the V−O bond (from $VO_4^{3-}$ groups) and the Y−O bond,[28] respectively. The presence of the two peaks indicates that yttrium vanadate has formed, in good agreement with the result from XRD. Furthermore, in comparison to that of the precursor, the absorption peak of the V−O bond in the hydrothermal product is slightly blue-shifted, which indicates that the V−O bond strength is stronger than that before hydrothermal treatment because of the improvement of the crystallinity. The broad absorption band at 3400 $cm^{-1}$ corresponds to the OH groups of $H_2O$ absorbing to the surface of the $YVO_4:Er^{3+}$ nanocrystals.[29] The peaks at 1367 and 1516 $cm^{-1}$ in the hydrothermal sample and the peaks at 1396 and 1576 $cm^{-1}$ in the precursor sample are assigned to vibrations of the carboxylate anion in the citrate,[29,30] which proves the presence of the citrate ligands on the surface of the nanoparticles. The positions of these two bands were

(26) Broch, Z. Z. *Phys. Chem. Abt. B* **1932**, *20*, 345.
(27) Wyckoff, R. W. G. *Crystal Structures*; Interscience: New York, 1963.
(28) Hirano, S.; Yogo, T.; Kikuta, K.; Sakamoto, W.; Koganei, H. *J. Am. Ceram. Soc.* **1996**, *79*, 3041.
(29) Lin-Vien, D.; et al. *The Handbook of IR and Raman Characteristic Frequencies of Organic Molecules*; Academic Press: New York, 1991; p 137.
(30) Wang, Y.; Teng, X. W.; Wang, J. S.; Yang, H. *Nano Lett.* **2003**, *3*, 790.

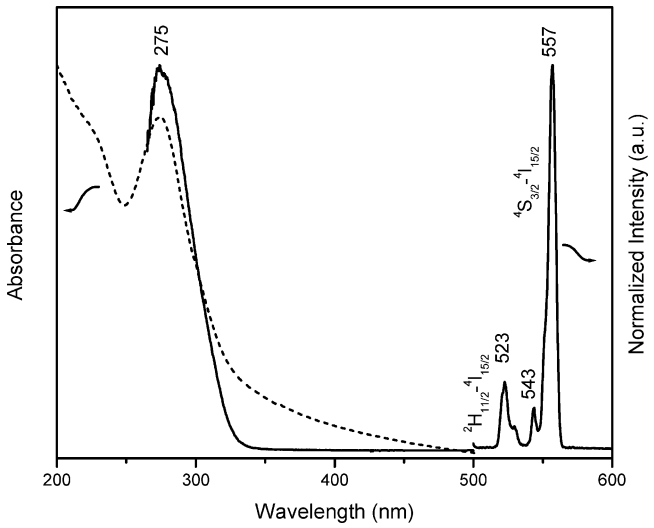


**Figure 4.** UV−vis absorption (dashed line), luminescence ($\lambda_{exc} = 280$ nm), and excitation ($\lambda_{em} = 523$ nm) spectra of a dilute ($2 \times 10^{-4}$ M) colloidal solution of nanocrystalline $YVO_4:Er^{3+}$.

sensitive to the chemical compositions of the nanoparticle surfaces.[31] In addition, the FT-IR spectrum for the hydrothermal product (Figure 3b) shows that the two weak bands at 3741 and 1646 $cm^{-1}$, which are assigned to OH stretching vibration modes for coordinated water,[32] and the two weak bands at 2925 and 2851 $cm^{-1}$ correspond to the asymmetrical and symmetrical stretching vibration modes, respectively, of the $CH_2$ group.[33,34] In the case of the precursor sample, weak bands peaking at 1253 and 1074 $cm^{-1}$ are assigned to the C−O stretching bands of the citrate.[29] These FT-IR spectra results reveal that the hydrothermal treatment decreases the quantity of the nanocrystal surface ligands.

**Optical Properties of $YVO_4:Er^{3+}$ Nanocrystals.** The absorption, emission, and excitation spectra of a colloidal solution of nanocrystalline $YVO_4:Er^{3+}$ are shown in Figure 4. The absorption peak at 275 nm is attributed to charge transfer from the oxygen ligands to the central vanadium atom inside the $VO_4^{3-}$ groups. The high absorption coefficient (absorption coefficient $\alpha_{max} = 2 \times 10^5$ $cm^{-1}$) indicates an optically allowed transition within the vanadate group.[26] The excitation spectrum exhibits a peak shape practically identical to that for the absorption spectrum. Upon UV ($\lambda = 280$ nm) excitation, $Er^{3+}$-doped $YVO_4$ nanocrystals exhibit strong green luminescence caused by f−f transitions in the erbium ions. The main emission bands at 523 and 557 nm are associated with the $^2H_{11/2} \rightarrow {}^4I_{15/2}$ and $^4S_{3/2} \rightarrow {}^4I_{15/2}$ transitions of the $Er^{3+}$ ions in the $D_{2d}$ site, respectively. The $Er^{3+}$ ions have no absorption at the excitation wavelength of ~280 nm. Therefore, it is clear that the erbium emission of nanocrystals originates from the energy transfer of the vanadate-group excitation. The relevant energy-transfer process is depicted in Figure 5. The emission intensity of the $Er^{3+}$ depends on the absorption of a host and energy-transfer efficiency from the host to the $Er^{3+}$ ions. For the $YVO_4$ host, the Y−O bond has strong absorption of relatively short wavelength UV light and the V−O bond absorbs relatively long-wavelength UV light. Furthermore, we may expect a marked influence of the angle formed by the central absorption atom, oxygen ion, and RE ion on the efficiency of the energy transfer. From magnetic studies, superexchange between paramagnetic ions is also dependent on the angle of paramagnetic ion, oxygen ion, and paramagnetic ion. This interaction is strong if the angle is 180° ($\sigma$-bonding) and becomes considerably weaker for 90° ($\pi$-bonding).[35] The V−O−Y angle of 170°, which makes the $\sigma$-bonding overlap almost optimal, induces an efficient energy transfer from $VO_4^{3-}$ to $Er^{3+}$ ions.[36]

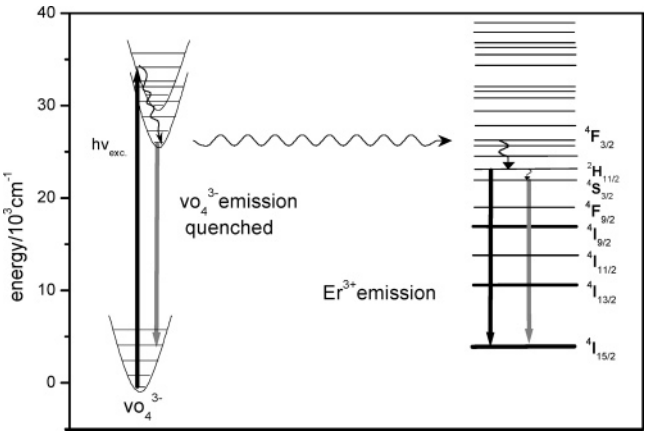


**Figure 5.** Part of the energy-level scheme of $YVO_4:Er^{3+}$. The excitation, emission, and energy-transfer processes are indicated.

**Upconversion Emission Spectroscopy.** Continuous wave excitation with a 980 nm semiconductor laser at room temperature leads to the upconversion emission of $Er^{3+}$-doped $YVO_4$ nanocrystals in the visible region, as shown in Figure 6 along with the energy level diagram of the $Er^{3+}$ ions. The nanoparticles showed a more intense visible upconversion emission after hydrothermal treatment. The peaks were assigned to the following transitions: the green emission in the 520−570 nm region is assigned to the ($^2H_{11/2}$, $^4S_{3/2}$) $\rightarrow {}^4I_{15/2}$ transition and the red emission in the 650−670 nm region is assigned to the $^4F_{9/2} \rightarrow {}^4I_{15/2}$ transition for the $Er^{3+}$ ion in the $D_{2d}$ site of nanocrystalline $YVO_4$.

Upconversion processes of the solid materials containing RE ions have been widely investigated.[37,38] Usually, it can be treated as an energy-transfer upconversion (ETU) process and excited-state absorption (ESA). To better understand the populating mechanism of the $^2H_{11/2}$, $^4S_{3/2}$, and $^4F_{9/2}$ excited states following NIR irradiation, we measured the upconversion luminescence intensities of the green and red emissions as a function of the excitation power (Figure 7). For an upconversion process, the intensity of the upconversion luminescence ($I_{UC}$) is proportional to some power $n$ of the incidence pump laser intensity ($I_{Pump}$) as follows

$$I_{UC} \propto {I_{Pump}}^n \text{ with } n = 2, 3, ... \quad (2)$$

where $n$ is the number of pump photons absorbed per short-

(31) Wang, W.; Chen, X.; Efrima, S. *J. Phys. Chem. B* **1999**, *103*, 7238.
(32) Hiramatsu, H.; Osterloh, F. E. *Langmuir* **2003**, *19*, 7003.
(33) Clothup, N. B.; Daly, L. H.; Wiberley, S. E. *Introduction to Infrared and Raman Spectroscopy*, 2nd ed.; Academic Press: New York, 1975; Chapters 5, 7, and 9.
(34) Socrates, G. *Infrared Characteristic Group Frequencies*; Wiley: New York, 1980.
(35) Goodenough, J. B. *Magnetism and the Chemical Bond*; Interscience Publishers: New York, 1963.

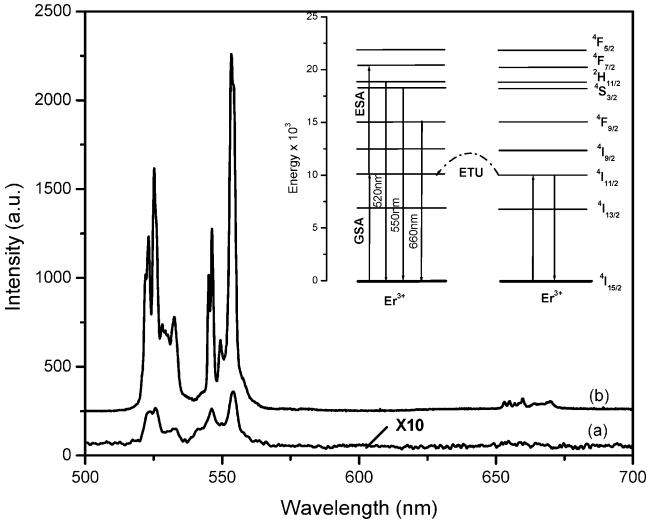


**Figure 6.** Upconverted fluorescence emission spectra of the 2.0 mol % $Er^{3+}$-doped $YVO_4$ nanocrystals ($\lambda_{exc}$ = 980 nm) (a) before and (b) after hydrothermal treatment. Inset: Schematic representation of the ground-state absorption (GSA), excited-state absorption (ESA), and energy-transfer upconversion (ETU) mechanisms.

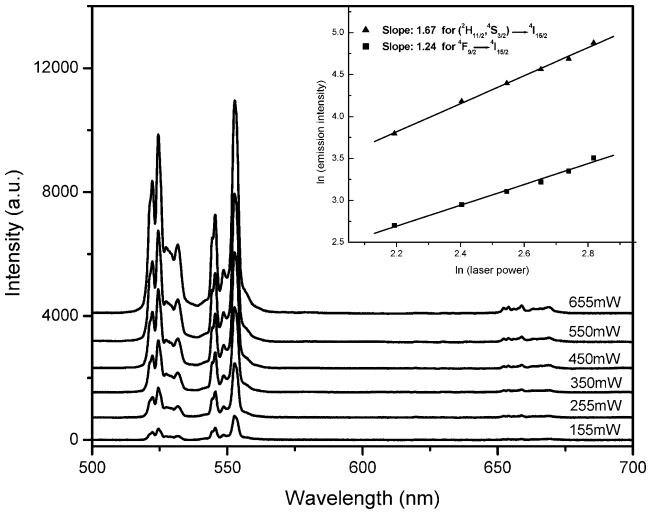


**Figure 7.** Power dependence of the upconverted luminescence in nanocrystalline $YVO_4$:$Er^{3+}$ following excitation with 980 nm. Inset: Graph of $\log(I_{UC})$ vs $\log(I_{Pump})$ for the sample.

wavelength photon emitted. According to this relation, a slope $n$ of the $\ln(I_{UC})$ vs $\ln(I_{Pump})$ curve can be determined. A straight line created by fitting the data points yielded slopes of 1.67 and 1.24 for the ($^2H_{11/2}$, $^4S_{3/2}$) → $^4I_{15/2}$ and $^4F_{9/2}$ → $^4I_{15/2}$ transitions, respectively, in all samples (Figure 7). From the fitting, we can confirm that the upconversion mechanism corresponding to green and red emissions occurs via a two-photon process. Figure 6 shows the upconversion mechanisms proposed for visible emission of the $Er^{3+}$ in the $YVO_4$ nanocrystals. As mentioned above, the dominant mechanisms of the green and red emissions are ETU and ESA. The mechanism for ESA is comparatively simple. The laser light excites the $Er^{3+}$ ion to the $^4I_{11/2}$ level, and a second photon from the incident laser beam brings the ion to the $^4F_{7/2}$ level, because this state is unstable; the electron then rapidly decays nonradiatively to the $^2H_{11/2}$ and $^4S_{3/2}$ levels. Alternatively, after the initial excitation, the $Er^{3+}$ ion nonradiatively decays down to the $^4I_{13/2}$ level and then populates the $^4F_{9/2}$ level by the absorption of a second 980 nm wavelength photon. In the ETU mechanism, two close $Er^{3+}$ ions are simultaneously excited to the $^4I_{11/2}$ level. One $Er^{3+}$ ion transfers its energy to the neighboring ion, leaving it in the higher excited state $^4F_{7/2}$, and nonradiatively decays back to the ground state. However, two independent processes, ETU and ESA, can occur concomitantly. When the dopant concentration is 0.5 mol % or less, the energy transfer between dopant ions can be ignored. It is well-known that the energy transfer can play an important role in the contribution to the upconversion luminescence when the dopant-ion concentration reaches a certain level.

It is obvious that the upconversion process in the samples before hydrothermal treatment is far less efficient than that after hydrothermal treatment. This increase in luminescence for the hydrothermal sample is attributed to the decrease in the multiphonon relaxation of the excited levels of Er because of a small number of ligand coordinates. As described above, the IR spectra show the presence of carboxylate (1350−1550 $cm^{-1}$) and hydroxyl (3400 $cm^{-1}$) groups on the surface of the nanoparticles, and the amount of carboxylate and hydroxyl in the hydrothermal product is evidently reduced. The populations of the intermediate levels, from which a part of the excited ions can be re-excited to the upper emitting levels by ESA, are substantially impacted by the nonradiative decay rate, which increases as the lattice phonon energy increases. The highest available phonon energy affects the upconversion efficiency, which is primarily determined by the populations of the intermediate levels. The excitation populations of the intermediate levels and the quantum efficiency of the emitting levels of $Er^{3+}$ in a host crystal with a lower phonon energy are undoubtedly higher than those in a crystal with a higher phonon energy. On the other hand, a hydrothermal treatment could induce an aggregation of the nanoparticles, a process in which they combine to form larger particles. In this case, as the spectroscopy of the nanocrystalline material is particle-size dependent, the smaller particles have a relatively larger surface-to-volume ratio, resulting in much more light scattering at the surfaces; thus, the luminescent efficiency is lower. Therefore, the upconversion intensity of the samples after hydrothermal treatment is evidently increased because of the decrease in the number of ligands and the larger particle size.

Figure 8 displays the measured temperature dependence of the green and red upconversion emissions for the hydrothermal sample under 980 nm excitation. At 77 K, transition to the ground state originating from the $^2H_{11/2}$ level was not observed, whereas both the emissions of the $^4S_{3/2}$ → $^4I_{15/2}$ and $^4F_{9/2}$ → $^4I_{15/2}$ transitions were clearly detected. However, as the temperature increased to 111 K, the hot band corresponding to the $^2H_{11/2}$ → $^4I_{15/2}$ transition was very weak. Following an increase in the measured temperature, we observed an increase in the luminescence intensity of the $^2H_{11/2}$ → $^4I_{15/2}$ transition and a decrease in the $^4S_{3/2}$ →

(36) Huignard, A.; Buissette, V.; Laurent, G.; Gacoin, T.; Boilot, J. P. *J. Phys. Chem. B* **2003**, *107*, 6754.
(37) Bloembergen, N. *Phys. Rev. Lett.* **1959**, *2*, 84.
(38) Chivian, J. S.; Case, W. E.; Eden, D. D. *Appl. Phys. Lett.* **1979**, *35*, 124.

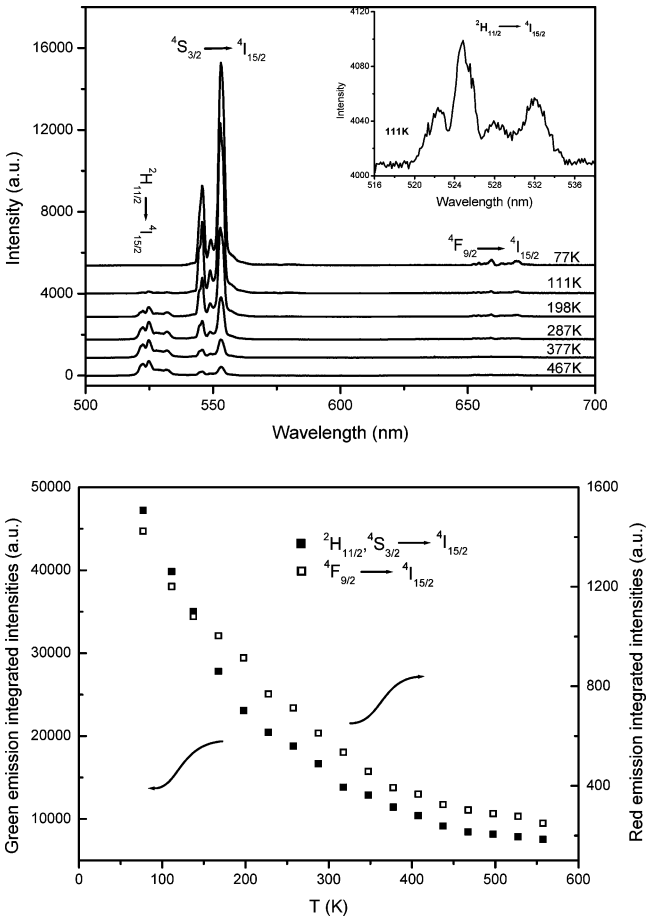


**Figure 8.** Top: Measured temperature dependence of the upconversion emission spectra for the hydrothermal sample at a fixed excitation power of 350 mW under 980 nm. Inset: Magnification of the $^2H_{11/2} \rightarrow {}^4I_{15/2}$ emission at 111 K. Bottom: Intensities of the green and red upconversion emissions as a function of temperature for a fixed excitation power of 350 mW at 980 nm.

$^4I_{15/2}$ intensity, and the former transition was dominant compared with the latter one up to 377 K. This occurs because the $^4S_{3/2}$ state is the feeding level for the $^2H_{11/2}$ level, and as a result of the $^2H_{11/2}$ population, the $^4S_{3/2}$ level is depopulated. It is noted that the green and red emission intensities of the ($^2H_{11/2}$, $^4S_{3/2}$) $\rightarrow$ $^4I_{15/2}$ and $^4F_{9/2} \rightarrow {}^4I_{15/2}$ transitions, respectively, decrease with increasing temperature, and both decrease nonlinearly. At 77 K, both the green and red upconversion emission intensities are about 5 times greater than those at 500 K.

Finally, it is possible to predict the relative populations of the $^4S_{3/2}$ and $^2H_{11/2}$ levels using a three-level model comprising the former (level 2), the latter (level 3), and the $^4I_{15/2}$ ground level (levle 1). The thermalization of the $^2H_{11/2}$ level may be expressed by the following equation[39]

$$\frac{I_3}{I_2} = A \exp\left(\frac{-\Delta E_{32}}{kT}\right) \tag{3}$$

where $I_3$ and $I_2$ are the integrated emission intensities of the $^2H_{11/2} \rightarrow {}^4I_{15/2}$ and $^4S_{3/2} \rightarrow {}^4I_{15/2}$ transitions of the $Er^{3+}$ ion,

(39) Shinn, M. D.; Sibley, W. A.; Drexhage, M. G.; Brown, R. N. *Phys. Rev. B* **1983**, *27*, 6635.

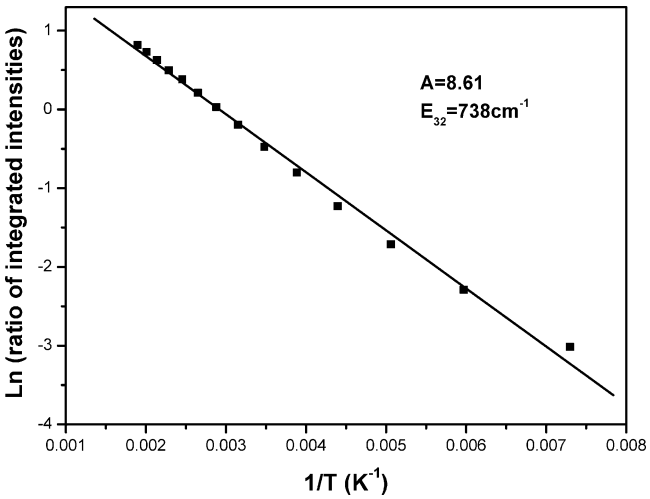


**Figure 9.** Logarithm of the integrated intensity ratio of the $^2H_{11/2} \rightarrow {}^4I_{15/2}$ to $^4S_{3/2} \rightarrow {}^4I_{15/2}$ transitions as a function of the inverse of the absolute temperature ($1/T$).

respectively, $\Delta E_{32}$ is the energy gap between the $^2H_{11/2}$ and $^4S_{3/2}$ levels, $k$ is Boltzmann's constant, and $T$ is the absolute temperature. The preexponential factor, $A$, is given by the following equation

$$A = \frac{W_{R3} g_3 h\nu_3}{W_{R2} g_2 h\nu_2} \tag{4}$$

where $W_{R3}$ and $W_{R2}$ are the radiative probabilities of two transitions, $g_3$ and $g_2$ are the $(2J + 1)$ degeneracies of levels 3 and 2, respectively, and $h\nu_3$ and $h\nu_2$ are the photon energies of the respective transitions from levels 3 and 2 to level 1. The calculated values of $\ln(I_3/I_2)$ as a function of $1/T$ were fitted using a straight line; from the slope, an energy gap of 738 $cm^{-1}$ was obtained (Figure 9). This value is in good agreement with the difference between the lowest-energy $^2H_{11/2}$ Stark level and the highest-energy $^4S_{3/2}$ Stark level determined from the luminescence spectra ($\Delta E_{32}$ = 733 $cm^{-1}$). The $A$ parameter is 8.6, which would suggest that the radiative transition probability $W_{R3}$ is greater than $W_{R2}$.

## Conclusion

Powders and colloids of $Er^{3+}$-doped $YVO_4$ nanoparticles were prepared using the simple method mentioned above. The nanoparticles with a diameter of 35 nm after hydrothermal treatment have a high crystallinity and can redisperse in water because of the presence of citrate ligands. Upon UV excitation of the host, the energy transfer to the $Er^{3+}$ ions occurs and the characteristic luminescence of the f−f transitions is observed. The green and red upconversion emissions were observed from the powders of the $Er^{3+}$-doped particles excited by 980 nm radiation. We have shown that the overall upconversion emission intensities depend on the multiphonon relaxation and particle size. In addition, we discuss thermal behavior of a hot band from the $^2H_{11/2} \rightarrow {}^4I_{15/2}$ transition for the $Er^{3+}$ ions in the $YVO_4$ nanocrystals; green upconversion emission intensity decreases with an increase in temperature. Therefore, the $YVO_4:Er^{3+}$ nanocrystals could be useful as biological labels because they

are water-soluble and biocompatible. Further studies for improving the size control and studying the surface modifying and grafting of particles for biological applications are on the way.

**Acknowledgment.** The authors gratefully acknowledge the financial support of the Major Foundation of the Chinese Academy of Sciences (kjcxw2−*sw*−h12−02).

CM051971M